Applied Energy 391 (2025) 125938

Contents lists available at ScienceDirect

Applied Energy

journal homepage: www.elsevier.com/locate/apenergy

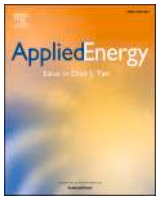

Electrolytic hydrogen in a large-scale decarbonized grid with energy reservoirs: An assessment of carbon intensity and integrity

Carlos E. Driemeier [a,*], Giovana C. Tonon [a], Mateus F. Chagas [a], Gabriel P. Petrielli [a], Daniele S. Henzler [a], Luísa C.M. Gomes [a], Bruno E. Limeira [b], Thayse A.D. Hernandes [a], Edvaldo R. Morais [a]

[a] Brazilian Biorenewables National Laboratory (LNBR), Brazilian Center for Research in Energy and Materials (CNPEM), Campinas, Brazil
[b] Technology Unit (DAT), Brazilian Center for Research in Energy and Materials (CNPEM), Campinas, Brazil

HIGHLIGHTS

- Case study of low-carbon e-H_2 production connected to a highly decarbonized grid.
- Comprehensive life cycle assessment of the e-H_2 carbon intensities.
- Critical analysis of electricity sourcing requirements to ensure carbon integrity.
- Flexible e-H_2 temporality due to grid-based energy storage and complementarities.

GRAPHICAL ABSTRACT

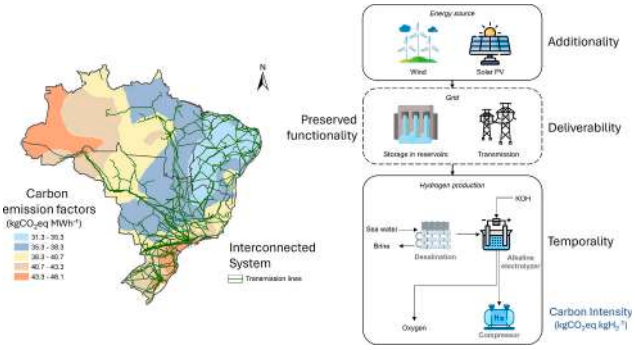

ARTICLE INFO

Keywords:
Alkaline electrolysis
Life cycle assessment
GWP
Time-matching
Green hydrogen

ABSTRACT

Electrolytic hydrogen (e-H_2) is under scrutiny worldwide to become a primary vector for decarbonization. Production of e-H_2 in Brazil is a unique case study because of the singularities of the electricity grid, which has a continental scale, is highly decarbonized (93 % renewables in 2023), and incorporates substantial energy storage (210 TWh) and dispatch flexibility (circa 50 GW) in hydro reservoirs. In this distinctive context, this study evaluates the carbon intensity (quantified through a cradle-to-gate life cycle assessment) and the requirements to ensure the carbon integrity of grid-connected e-H_2 production. The study gathers inventories of solar and wind energy systems and alkaline electrolyzers. It also presents georeferenced modeling of carbon emission factors for solar and wind energy, along with hourly simulations of grid-connected e-H_2 production. Carbon intensities within 2.9–4.0 $kgCO_2eq\ kgH_2^{-1}$ are calculated with solar energy and as low as 1.0 $kgCO_2eq\ kgH_2^{-1}$ with wind energy. Energy sourcing from the best wind sites leads to the lowest carbon intensities, even if adding the impacts of long-distance (2000 km) transmission. Simulation of e-H_2 production with wind energy assisted by energy storage in hydro reservoirs shows that electrolysis at a high capacity factor (≈90 %) is possible without impacting grid emissions and reservoir functionality. This result demonstrates that the requirement of hourly matching between additional energy generation and consumption is unsound for e-H_2 production in a grid rich in

* Corresponding author.
E-mail address: carlos.driemeier@lnbr.cnpem.br (C.E. Driemeier).

https://doi.org/10.1016/j.apenergy.2025.125938
Received 13 January 2025; Received in revised form 1 April 2025; Accepted 11 April 2025
Available online 22 April 2025

renewables. Instead, the temporality of electrolysis must consider the permissible temporal unmatching enabled by the grid-based energy storage and the complementarity between the legacy and the additional renewable sources.

1. Introduction

The falling costs and remarkable growth of solar and wind energy, combined with the need for scalable solutions to mitigate greenhouse gas (GHG) emissions, have created the foundations for the large-scale deployment of electrolytic hydrogen (e-H_2), often named green hydrogen [1,2]. Low-carbon e-H_2 is recognized as a potential vector to defossilize hard-to-abate sectors such as the steel and chemical industries and fuels for long-haul transportation [3,4]. A surge of investment announcements and governmental incentives has motivated a deeper analysis of the low-carbon credentials of e-H_2 [5,6]. Grid connection offers multiple benefits to e-H_2 production, but ensuring environmental integrity requires evaluating the systemic impacts that e-H_2 production promotes in the electricity grid, avoiding unintended GHG emissions [7–9].

The carbon integrity of grid-connected e-H_2 has been framed based on three requirements for electricity sourcing: additionality, deliverability, and time matching [8]. Additionality aims to ensure that the electrical energy for e-H_2 is obtained from new renewable capacity. Distinct interpretations of additionality have been proposed, depending on whether clean energy for e-H_2 and non-H_2 uses is considered in direct competition [7]. Moreover, the implementation of additionality has been framed based on distinct contractual instruments (power purchase agreements and energy attribute certificates) and criteria for the new capacity, such as the installation date and the lack of relationship with other clean energy mandates or incentives [8,9]. As for deliverability, it aims to ensure that the points of energy generation and consumption are adequately connected, avoiding transmission constraints that may prevent the delivery of clean energy to e-H_2 production [8].

The time-matching requirement establishes a timescale over which the additional energy generation must equal the consumption for e-H_2 production. Yearly matching is the most straightforward requirement. However, it may result in induced GHG emissions in the grid due to fossil power sources needed to meet e-H_2 consumption when there is an insufficient renewable generation (i.e. when the sun is not shining and the wind is not blowing). Therefore, shorter timescales are prescribed to avoid such induced emissions. Hourly matching, a practical implementation of simultaneity, has become widely accepted as an ultimate time-matching requirement. Hourly matching has been incorporated into the language of the research literature [7–9] and the e-H_2 regulations that include the EU Delegated Act [10] and the US Inflation Reduction Act [11]. However, the stringency of hourly matching has been criticized as a source of economic inefficiencies, promoting energy and electrolyzer over-capacities and, thus, higher e-H_2 production costs compared to more flexible approaches to the temporality of electrolysis [12,13]. Moreover, the rationale for a stringent simultaneity requirement has been conceived primarily for grids still dominated by fossil energy, motivated by concerns about induced GHG emissions from fossil power sources.

The Brazilian electrical system has evolved over decades to integrate high shares of renewable energy [14], offering a unique case study to test and possibly reframe the requirements for low-carbon e-H_2. The National Interconnected System (SIN – *Sistema Interligado Nacional*) comprises more than 170,000 km of transmission lines to integrate renewable energy on a continental scale (Brazilian continental territory except for parts of the Amazon) and counts with substantial energy storage in hydro reservoirs (210 TWh; ≈4 months of energy generation) [15]. In addition, the SIN is highly decarbonized, with a share of renewable energy consistently above 70 % in the last 20 years, reaching 93 % in 2023 [16]. Such share of renewables, geographic coverage, and energy storage anticipate a set of characteristics that other grids worldwide may acquire as they decarbonize. Moreover, a global comparison indicated that Brazil may reach the lowest e-H_2 production costs [17], which may transform the country into a major e-H_2 powerhouse. Recent studies evaluated the potential of e-H_2 production in Brazil using hydroelectric spilled energy [18] and the techno-economics of e-H_2 produced with a combination of solar and wind energies under an hourly matching requirement [19]. However, the current literature on e-H_2 does not appreciate in detail the specificities of the GHG emissions of e-H_2 connected to a large-scale grid rich in renewables. Thus, the Brazilian case offers a unique perspective to position the country's specificities and learn the general lessons from its large-scale low-carbon grid.

This work investigates the carbon intensity and the requirements to ensure the carbon integrity of grid-connected e-H_2 production. A unique perspective is achieved by examining the Brazilian case, with grid-connected e-H_2 powered by additional solar and wind energy. The uniqueness of the analysis stands because the large-scale, highly decarbonized grid is already an observable reality, not a model of a possible future. In this context, the carbon intensities of e-H_2 production are calculated through a cradle-to-gate life cycle assessment based on georeferenced data on solar and wind resources and inventories of solar and wind energy systems and alkaline electrolyzers. Beyond the direct emissions in energy generation, the life cycle assessment accounts for the embodied emissions associated with the capital goods used for energy generation, transmission, and electrolysis facility. In addition, the carbon integrity of grid-connected e-H_2 production is examined by accounting for the data and fundamentals of the grid operation and simulating grid-connected e-H_2 production. By learning from the peculiar characteristics of the Brazilian grid, this work aims to illuminate how the additionality, deliverability, and temporality requirements should be reframed for an electricity grid rich in renewables.

2. Methods

2.1. Life cycle assessment

The system boundaries to evaluate the life cycle carbon intensity of e-H_2 are illustrated in Fig. 1. All the life cycle stages from resource extraction (cradle) to factory gate are included within the system boundaries, i.e., a cradle-to-gate life cycle assessment. The system contemplates wind and solar energy generation, the use of the grid to connect energy generation and consumption, and e-H_2 production, which encompasses seawater desalination by reverse osmosis, alkaline water electrolysis, and H_2 compression. The final phases of transportation, use, and disposal of H_2 or its derived products are not included. The functional unit of energy generation is one MWh at the point of generation. The functional unit for the life cycle assessment is one kgH_2 at 70 bar. Oxygen is considered a by-product of the process with no allocation of impacts. Carbon intensity was calculated using the IPCC 2021 GWP100 V1.02 life cycle assessment method. Mass and energy balances were calculated in spreadsheets to inform the life cycle inventories. The SimaPro 9.5® software and the ecoinvent 3.9.1® database [20,21] were used for the life cycle assessment.

The carbon emission factors of solar and wind energy were calculated from the footprints for mounted solar panels of the single-crystal silicon technology (373.5 $kgCO_2eq\ m^{-2}$) and a 1.65 MW wind turbine (1276 $tCO_2eq\ turbine^{-1}$). Georeferenced emission factors ($kgCO_2eq\ MWh^{-1}$) were calculated by dividing the carbon footprints of the solar and wind systems by the respective energy productions during their service life (25 years). The solar and wind energy system datasets are

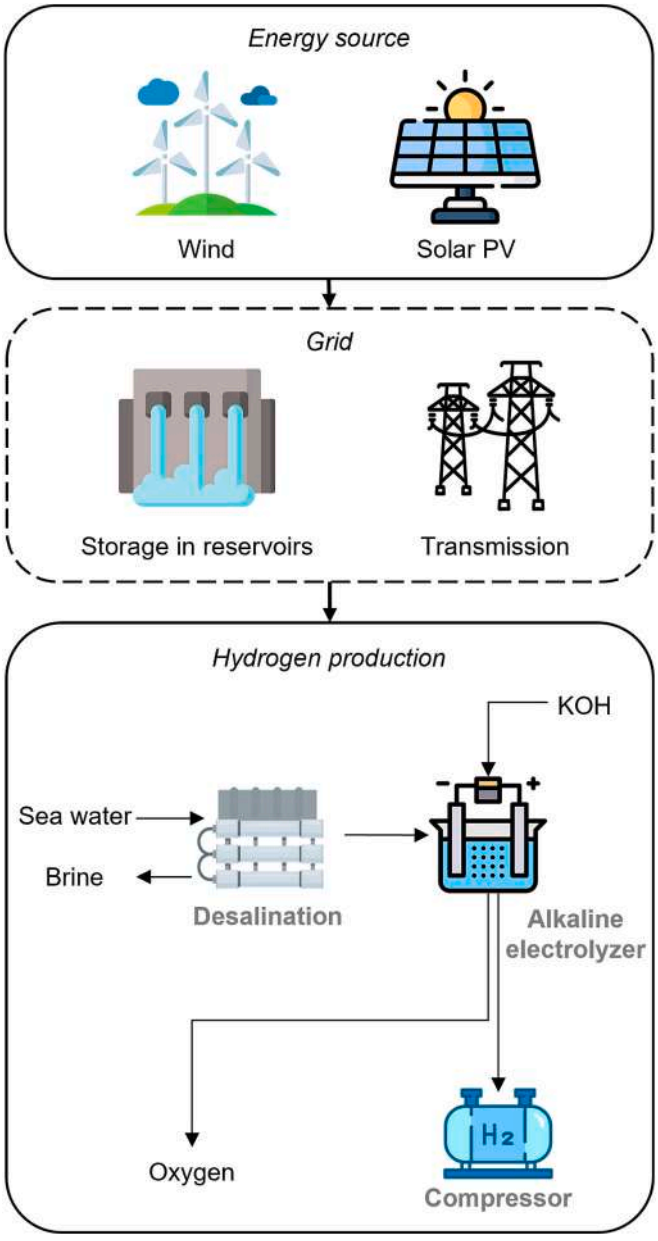

Fig. 1. Illustration of the system boundaries used in the life cycle assessment of electrolytic hydrogen.

provided in the **Supplementary Material sections 1.1 and 1.2**, **Tables S1–4**.

Energy storage in the existing hydro reservoirs was assumed to allow time shifts between energy generation and consumption without the net addition of impacts. This assumption was submitted to restrictions to preserve hydropower and reservoir functionality and avoid the dispatch of fossil power plants. An alternative energy storage approach using a utility-scale Li-ion battery was analyzed to contrast with the use of the existing hydro reservoirs. Details of the battery analysis are given in the **Supplementary Material section 1.3**.

Electricity transmission impacts accounted for infrastructure and energy losses. Two scenarios of electricity transmission were considered: (i) The mean impacts of transmission in the SIN, with energy loss of 6 % and an infrastructure emission factor of 2.83 $kgCO_2eq\ MWh^{-1}$ [20,21]. (ii) The mean impacts (i) plus a high-voltage direct current (HVDC) transmission line with specifications (800 kV, 2000 km) representative of the contracted expansion (Graça Aranha – Silvania line) for transmission of new renewable energy from the north-northeast to central Brazil. The HVDC line considers energy loss of 5 %, infrastructure emission factor of 190 $kgCO_2eq\ MW^{-1}\ km^{-1}$ [22], service life of 40 years, and capacity factors equal to the ones of e-H_2 production. Details of the transmission scenarios are given in the **Supplementary Material section 1.4**.

The e-H_2 production system was modeled to calculate the impacts per kgH_2. This e-H_2 production system was dimensioned for 20 t of H_2 per day. Desalination by reverse osmosis assumed consumption of 4.4 kWh per cubic meter of clean water produced and a recovery rate of 40 % [23]. Alkaline electrolysis assumed a commercial electrolyzer efficiency (5 kWh Nm^{-3}). Energy consumption for H_2 compression was calculated considering an inlet temperature of 305.15 K, an inlet pressure of 20 bar, and a required outlet pressure of 70 bar. With these assumptions, the total specific energy consumption was 60.7 kWh kgH_2^{-1}. The footprint of the e-H_2 production system was calculated from an inventory based on Gerloff [24]. The electrolysis system was assumed to have a service life of 6.67 years for the electrolyzer stacks and 20 years for the balance of plant (BoP) [24]. Details of the electrolyzer and BoP datasets are given in the **Supplementary Material section 1.5**, **Tables S5–7**.

Leakage of H_2 was not considered in the calculated carbon intensities, which is a limitation of the study. Other uncertainties in the life cycle assumptions were considered in the sensitivity analysis given in the **Supplementary Material section 1.7, Figs. S1–3**. Moreover, the choices of technologies for the life cycle assessment had the following motivations. The solar and wind energy systems and the mean impact of energy transmission are representative of recent energy expansion and the current status of the transmission within the SIN. The HVDC transmission line is representative of the ongoing expansion of the transmission capacity to increase the delivery of solar and wind energy to the SIN. The alkaline electrolyzer is a mature commercial technology for an expected ramp-up of e-H_2 installations. The choice of seawater desalination by reverse osmosis aims to circumvent site-specific concerns about freshwater availability. As presented in the results section, the choices of water supply and e-H_2 compression have minute impacts on carbon intensity compared to electrolysis, thus not compromising the representativeness of the analysis.

2.2. Georeferenced generation of solar and wind energy

The wind speed data were obtained from the historical period (1960–2005) of the Brazilian Earth System Model (BESM), which comprises daily data of wind speed at 10 m and 100 m height in a grid cell of 0.2° × 0.2° (~22 km × 22 km) [25]. Solar radiation, air temperature, and relative humidity data were taken from Brazilian Daily Weather Gridded Data (BR-DWGD), a 0.1° × 0.1° (~11 km × 11 km) grid cell with daily data from 1961 to 2020 [26]. The daily averages of wind speed and solar radiation for each cell were obtained by calculating climatological normal using the last 35 years from each dataset. Based on historical data, a limitation of this approach is that it did not account for the alterations of solar and wind resources due to climate change. The final maps were based on the best spatial resolution by attributing wind speed from BESM to the BR-DWGD spatial grid.

The daily solar energy output per m^2 of mounted panel (E_{PV}) was calculated following Ma et al. [27]

$$E_{PV} = \eta_{PV}\, R, \tag{1}$$

where $\eta_{PV} = 21.5$ % is the solar system's efficiency, including panel and inverter efficiency, and R is the georeferenced global horizontal radiation (kWh m^{-2} day^{-1}) obtained from the BR-DWGD dataset. Solar capacity factors were calculated from the annual energy output referenced to the rated power for 1000 W m^{-2} irradiance.

The daily wind energy output per turbine E_{WT} (kWh) was calculated as

$$E_{WT} = d\, C_P(v_{hb})\, \frac{1}{2}\, \rho\, A_{RS}\, v_{hb}^3, \quad (2)$$

where d is the period of one day (h), $C_P(v_{hb})$ is the wind turbine power coefficient (%), ρ is the air density (kg m^{-3}), A_{RS} is the rotor swept area (m^2), and v_{hb} is the wind speed at hub high (m s^{-1}) [28]. v_{hb} at a hub high of 80 m was calculated from the wind speeds at 10 m and 100 m in the BESM dataset, using the wind shear coefficient for interpolation (**Eqs. S1–2**). ρ was calculated from monthly average pressure, temperature, and relative humidity obtained from the BR-DWGD dataset (**Eqs. S3–4**). A_{RS} and $C_P(v_{hb})$ were obtained from data from a representative wind turbine. Wind capacity factors were calculated from the annual energy output referenced to the nominal capacity of the model turbine. Noteworthy, using a model turbine not optimized for each site may underestimate the wind energy potential. Details of the wind energy calculation are given in the **Supplementary Material section 2**.

2.3. Characterization of the electricity grid

Data on the SIN was obtained from the National Electric System Operator (ONS – *Operador Nacional do Sistema Elétrico*). Data comprised energy generation, installed capacities, energy storage in the reservoirs, reservoir capacity, long-term means of streamflow energy in hydropower basins, projection of future installed capacity, and monthly mean capacity factors of solar and wind generation (the data sources are indicated in **Table S8**). Noteworthy, the long-term means of streamflow energy are utilized as reference by the ONS but do not account for resource alterations due to climate change. Additional data on hourly energy spot prices, georeferenced transmission lines, and solar and wind systems were obtained from other official sources. **Table S8** details the web-based data sources and the Portuguese-English translation of the SIN glossary. The analysis did not consider energy imports and exports (<8 % of the SIN energy).

Monthly and yearly data from the calendar year of 2023 was used to present the main characteristics of the SIN and its subsystems (N: North; NE: Northeast; SE-CO: Southeast-Centerwest; and S: South). The carbon emission factor from the grid energy was calculated based on the 2023 energy mix (**Table S9**). The seasonality of the renewable resources was characterized by the monthly long-term means (since 1931) of streamflow energy and the monthly mean capacity factors of solar (from May/2023 to Apr/2024) and wind generation (from Jan/2021 to Dec/2023).

2.4. Simulation of grid-connected e-H_2 production

Grid-connected e-H_2 production was simulated based on hourly energy generation in the SIN from 04/30/2023 to 04/29/2024. This one-year interval avoided the ONS methodology's discontinuity (by 04/29/2023) for distributed solar energy. All times were given in the BRT time zone. The simulations were conducted assuming unconstrained energy transmission within the SIN. This assumption is justified by the strong interconnections within the SIN, as evidenced by the high correlation coefficients ($r \geq 0.990$) between the hourly energy prices in the distinct SIN subsystems (**Fig. S4**).

The simulations assumed 1 GW of electrolyzer capacity. (An additional simulation with 5 GW electrolyzer capacity is presented in the Supplementary Material.) This magnitude of additional e-H_2 capacity acted as a significant perturbation to the existing SIN (base case). It aimed to reveal the response of the hydropower legacy, assumed to meet the hourly difference between energy generation and consumption within the system boundaries (Fig. 1). Noteworthy, the simulation of 1 GW capacity was unrelated to the 20 t of H_2 per day system described in section 2.1, which was modeled to determine the life cycle impacts per kgH_2. The hydro generation $Y_{s,t}$ (GW) of scenario s at the hour t was calculated as

$$Y_{s,t} = Y_{b,t} + C_{s,t} - G_{s,t}, \quad (3)$$

where $Y_{b,t}$ (GW) is the hydro ***generation*** in the SIN data (base case, no e-H_2 production), $C_{s,t}$ (GW) is the power consumption for e-H_2 production, and $G_{s,t}$ (GW) is the additional power generation from solar or wind. Eq. 3 considers that the hydropower legacy is the only flexible asset of the existing grid. Although the hydropower legacy is by far the dominant element of flexibility, neglecting the flexibility of other grid-connected assets is a simplifying assumption of the analysis.

Two scenarios were constructed with solar energy (S100 and S30) and two with wind energy (W100 and W90), as summarized in Table 1. All the scenarios required annual matching between additional energy generation and consumption, i.e.,

$$\sum_{t}^{year} G_{s,t} = \sum_{t}^{year} C_{s,t}. \quad (4)$$

The temporal profile $G_{s,t}$ was calculated to represent a constant power capacity with hourly generation profiles representative of the solar or wind portfolios connected to the SIN. To obtain this $G_{s,t}$, the observed solar or wind generation in the SIN was divided by the installed capacities, which grew steadily during the simulated year.

As for the energy consumption profiles $C_{s,t}$, scenarios S100 and W100 assumed constant power consumption of 1 GW, i.e., e-H_2 production continuously operating at full load (capacity factor CF = 100 %). Scenarios S30 and W90 were constructed to meet hydropower stress requirements. Scenario S30 assumed a daily operational program, with consumption ramping up at 9:00 (0.3 GW) and 10:00 (0.8 GW) to reach a plateau at 11:00–15:00 (1 GW) and then ramping down at 16:00 (0.8 GW) and 17:00 (0.3 GW). This daily program makes CF = 30 %. Scenario W90 assumed 1 GW of power consumption, except (*i*) in hours between 17:00 and 22:00 with wind generation below 1.08 times the annual mean, when the consumption is set to 0 GW, and (*ii*) in the hours before and after case (i) when the consumption is ramping down or up (0.5 GW). S30 and W90 are proof-of-concept scenarios, not the result of any optimization. In addition, the W90 scenario maintains 1 GW of power consumption in hours between 17:00 and 22:00 when wind generation is above 1.08 times the annual mean. This choice of threshold results in the W90 scenario having CF = 90 % accounted through the analyzed year.

2.5. Analysis of impacts on hydropower and hydro reservoirs

Since the simulations assumed that hydropower met the difference between additional power consumption for e-H_2 and generation by solar or wind (Eq. 3), the impacts on hydropower and hydro reservoirs were evaluated. Metrics of hydropower stress were analyzed in simulated hydro generation $Y_{s,t}$ compared to the base case $Y_{b,t}$. The minimum and maximum hydropower generation (in units of GW) and the maximum hydropower ramp (in units of GW h^{-1}) were calculated within each calendar week to evaluate a sample of hours of grid stress.

The impacts on hydro reservoirs in the annual cycle were assessed by the energy balance $EB_{s,t}$ (GWh) of scenarios S30 and W90. $EB_{s,t}$ was calculated by summing the differences between energy generation and consumption from 0:00 04/30/2023 up to time t,

$$EB_{s,t} = \tau \sum_{t'}^{t} \left(G_{s,t'} - C_{s,t'}\right). \quad (5)$$

Table 1
Scenarios used in the simulation of grid-connected e-H_2 production.

Scenario name	Energy source	Electrolyzer CF (%)	Electrolyzer operation
S100	solar	100	continuous
S30	solar	30	preprogrammed daylight hours
W100	wind	100	continuous
W90	wind	90	continuous, with shutdowns during peak demand hours with low wind

In Eq. 5, τ is the interval of 1 h for converting power (GW) to energy (GWh). The induced impact Δ_s that scenario s has on the utilization of energy storage in hydro reservoirs across the analyzed year was calculated by

$$\Delta_s = EB_{s,tmax} - EB_{s,tmin}, \quad (6)$$

where *tmax* and *tmin* are the times during the analyzed year when energy storage in the hydro reservoirs is maximum and minimum, respectively.

3. Results

3.1. Maps of carbon emission factors from solar and wind energy

Solar and wind resources depend on local environmental conditions. The maps of Fig. 2A–B express these variations as changes in capacity factors calculated for the solar and wind energy systems. The maps of Fig. 2A–B can be compared with previous georeferenced resource assessments, such as the Brazilian and the global atlases of solar and wind resources [29–32].

The solar capacity factors of Fig. 2A fall within 16.2–24.9 %, with the higher factors located in the northeast and the lowest in the south and northwest. For comparison, capacity factors would be within 14.6–26.0 % using the ranges of horizontal irradiation (3500–6250 Wh m^{-2} day^{-1}) from the Brazilian solar atlas [29]. In addition, the ONS data reports a mean capacity factor of 24 % for systems connected to the SIN. This number is close to the upper limit (24.9 %) of Fig. 2A and thus consistent with commercial systems exploiting the superior solar resources. In summary, despite methodological differences, the solar capacity factors of this work compare well with those reported in the solar atlases and the ONS data.

The map of Fig. 2B shows that the capacity factors of wind energy vary from zero to 45 %. In comparison, the mean capacity factor reported for commercial wind systems in the SIN is 41 % [15]. This number is close to the upper limit of Fig. 2B and thus consistent with utilizing the best wind sites in commercial systems. However, the absence of offshore wind in the model is a significant limitation, and the Brazilian and global wind atlases are more informative for estimating wind potentials near the shoreline [30,32]. Moreover, as mentioned in the methodology (section 2.2), using a model turbine tends to underestimate the wind potential, although still revealing the geographical patterns of wind resources.

The carbon emission factors ($kgCO_2eq$ MWh^{-1}) are inversely proportional to the solar and wind capacity factors because energy production is the denominator in calculating the emission factors. Therefore, the capacity and emission factor maps resemble each other if the color scale is inverted, as in Fig. 2. The calculated emission factors for solar energy are distributed within 31.3–48.0 $kgCO_2eq$ MWh^{-1} (Fig. 2C). This range is well aligned with international literature. For instance, Tawalbeh et al. [33] compiled emission factors from photovoltaics and reported 5–69 $kgCO_2eq$ MWh^{-1} considering a range of technologies and 30–46 $kgCO_2eq$ MWh^{-1} for the single-crystal silicon technology, the same technology modeled in this work. Moreover, an International Energy Agency (IEA) database reports photovoltaic life cycle emission factors within 27.4–45.5 $kgCO_2eq$ MWh^{-1} (interquartile range) and a median of 33.0 $kgCO_2eq$ MWh^{-1} [34]. Similarly, a report from the National Renewable Energy Laboratory (NREL) presents a median of 43 $kgCO_2eq$ MWh^{-1} [35].

As for wind energy, emission factors can be as low as 7.9 $kgCO_2eq$

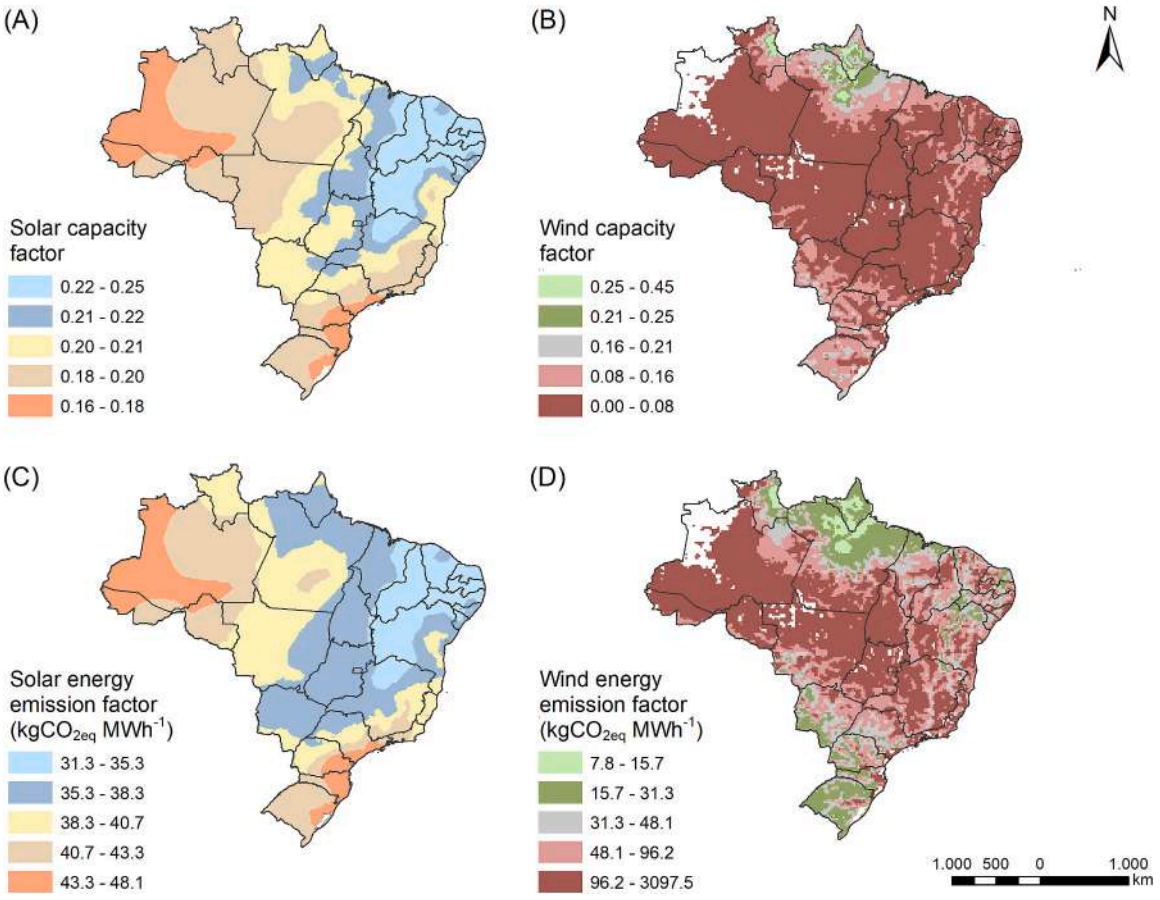

Fig. 2. Maps of modeled capacity factors of solar and wind energy generation (A, B) and the associated carbon emission factors (C, D). Unit conversion: 1 $kgCO_2eq$ MWh^{-1} = 0.28 gCO_2eq MJ^{-1}.

MWh^{-1} at the best wind sites and extremely high (~10^3 kgCO_2eq MWh^{-1}) at sites with scarce wind resources (Fig. 2D). In practice, only sites with superior wind resources will be commercially utilized. This work will consider the range 7.9–31.3 kgCO_2eq MWh^{-1} (green areas of Fig. 2D) with the remark that the most economical wind sites are near the bottom of this range. For comparison, the IEA database reports onshore wind emission factors within 8.6–13.9 kgCO_2eq MWh^{-1} (interquartile range) and a median of 10.6 kgCO_2eq MWh^{-1} [34], while the NREL report presents a median of 13 kgCO_2eq MWh^{-1} [35]. These comparisons show that the emission factors of this work align with the international literature. Furthermore, the results agree that wind energy tends to present a lower emission factor than solar photovoltaics.

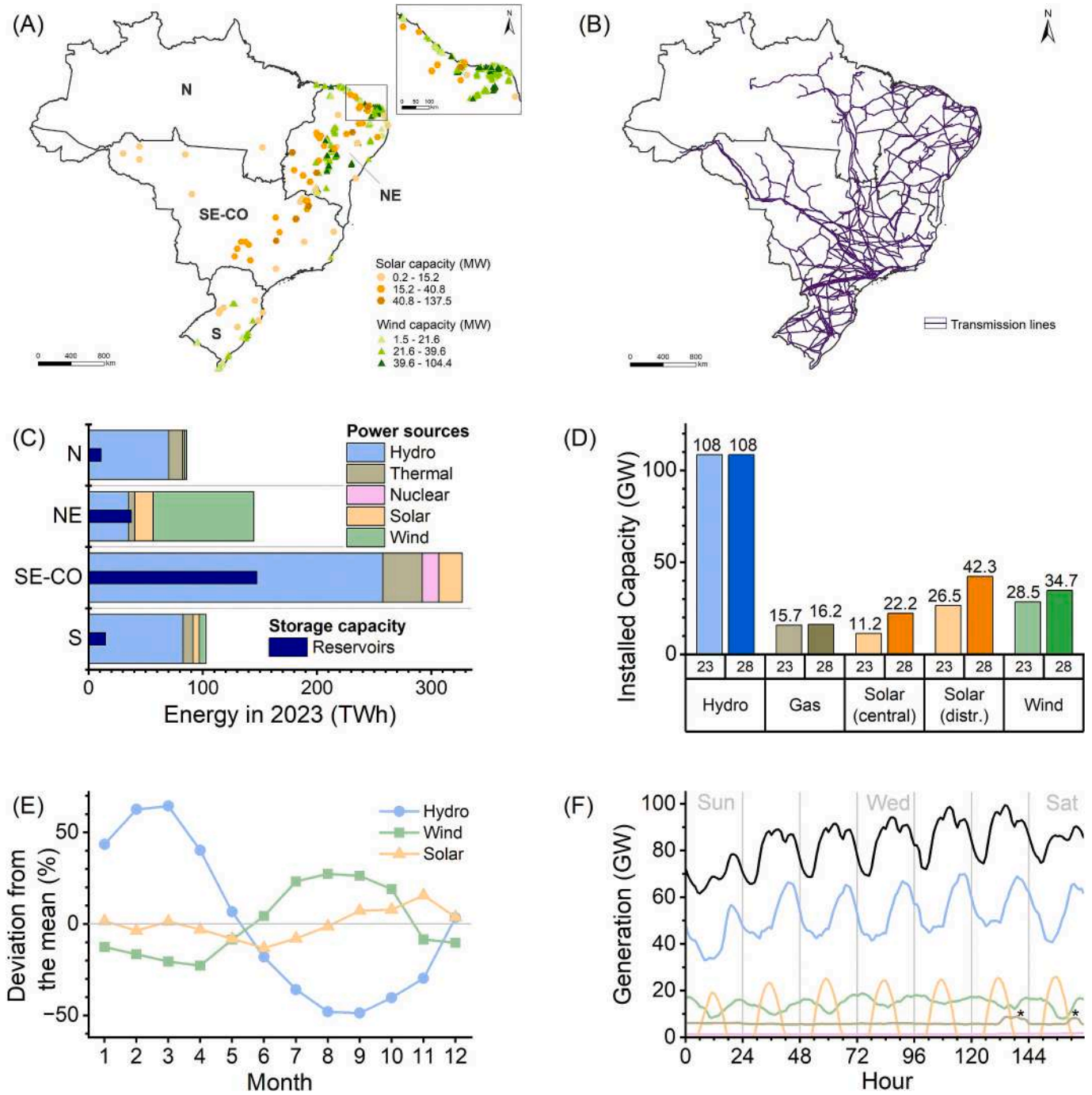

Fig. 3. Overview of the Brazilian national interconnected system (SIN). (A) Map indicating the regions of the four SIN subsystems (N, NE, SE-CO, and S) and the location of the installed capacity of centralized solar and wind installations. (B) Map of the current transmission lines. (C) Storage capacity in hydro reservoirs and energy generation by hydro, thermal, nuclear, solar, and wind sources in each subsystem in 2023. (D) Installed capacity of selected types of power sources by Dec/2023 and projected expansion by Dec/2028. (E) Seasonality of renewable resources presented as the monthly percentual deviations from the annual mean. Hydro seasonality was calculated from the historical long-term means of streamflow energy in the hydro basins. Wind and solar seasonalities were obtained from monthly capacity factors in recent years. (F) Hourly energy generation from hydro, thermal, nuclear, solar, and wind sources within an exemplary week (Sunday 12/10/2023 to Saturday 12/16/2023). The sum of all power sources is included (black line). Power from thermal peakers is marked (*).

3.2. Overview of the electricity grid

The consequential impacts of grid-connected e-H_2 depend on the characteristics of the electricity grid. The case of the Brazilian grid can be understood in more detail by examining the selected attributes of the SIN presented in Fig. 3.

The SIN subsystems (N, NE, SE-CO, and S) encompass most of the Brazilian territory (Fig. 3A–B) except for unconnected regions within the Amazon (N subsystem). Due to its geographic extension, the grid covers different climatic zones from the Equator to the southern tropics. The grid was developed as a hydrothermal system based on hydropower complemented by thermal energy. In recent years, solar and wind energy have been the main drivers of added capacity [14]. The installed solar and wind capacities (Fig. 3A) tend to be in the sites with superior resources, i.e., sites of higher capacity factors and lower emission factors (Fig. 2). Wind installations at the northeast shoreline (Fig. 3A, inset) indicate the superior resources thereat. Hydropower generated 445 TWh in 2023, corresponding to 67 % of the energy generation (Fig. 3C). The hydro reservoirs have a storage capacity of 210 TWh, corresponding to nearly 4 months of energy generation within the SIN. Substantial hydropower and reservoir capacity are found in the four subsystems, while wind energy is primarily located in the NE. Expansion of installed capacity until 2028 (Fig. 3D) is projected by the ONS (see **Table S8**) to come mainly from wind (28.5 → 34.7 GW), distributed solar (26.5 → 42.3 GW), and centralized solar (11.2 → 22.2 GW). Slight expansions are also projected for natural gas (15.7 → 16.2 GW) and small-scale hydro (7.2 → 7.8 GW, not discriminated in Fig. 3D), with no significant expansion of total hydro (108 → 108 GW).

As temporal profiles are considered, the seasonality of the energy sources (Fig. 3E) shows a remarkable complementarity between streamflow (hydro) and wind energies: the former peaks in February–March and the latter in August–October. Other authors have addressed this annual complementarity in more detail [36,37]. Monthly deviations from the mean for solar energy are approximately within ±15 %. Such minor deviations result from the preferential location of centralized solar power in regions with greater solar resources (Fig. 2A and Fig. 3A), primarily in equatorial and tropical zones. Moreover, the monthly maximum (November) and minimum (June) of solar energy are out of phase with the hydro and wind annual profiles (Fig. 3E).

The typical temporal patterns of power generation are shown in Fig. 3F within an exemplary week. Solar energy follows the expected daily profiles, while wind tends to complement solar with lower generation during daylight and higher at night. This wind-solar complementarity has also been investigated as a remarkable characteristic for integrating renewables into the SIN [38,39]. Hydro is the primary power source for load matching, with ranges (maximum-minimum) up to about 50 GW observed within a week. Thermal energy, which includes biomass and fossil fuels (**Table S9**), operates as a baseload, and so does nuclear. Moreover, thermal peakers (powered by natural gas, Diesel, and fuel oil) are occasionally dispatched to support hydro in load matching (see * mark in Fig. 3E). This graph thus delineates the two leading roles of fossil plants in the grid: (i) baseload to complement renewable energy in yearly timescales (especially important for energy security in years of draught) and (ii) peak power to complement hydro in the timescale of several hours.

In summary, the seasonal complementarities of hydro and wind (Fig. 3E), the daily complementarity of solar and wind (Fig. 3F), the energy storage in hydro reservoirs (Fig. 3C), and the load-matching flexibility of hydropower (Fig. 3F) are renewable assets of the existing grid that should be considered for additional e-H_2 production with optimal systemic efficiency.

3.3. Impacts of energy storage

Energy storage can significantly contribute to the economic costs and carbon intensity of e-H_2 production systems [1,5]. For example, the embodied emissions of the Li-ion battery storage evaluated in this work (**Supplementary Material section 1.3**) would contribute with an additional carbon intensity of 30.9 $kgCO_2eq$ per MWh delivered by the battery. It is essential to highlight that this is an order of magnitude greater than the mean impacts of transmission (2.83 $kgCO_2eq\ MWh^{-1}$), as detailed in **Supplementary Material section 1.4**. Moreover, this impact of battery storage is only slightly lower than the range calculated for solar energy generation (31.3–48.0 $kgCO_2eq\ MWh^{-1}$) and much higher than the results for the best wind energy sites (7.9 $kgCO_2eq\ MWh^{-1}$). Moreover, the carbon intensity of battery storage calculated here is within the range (9–135 $kgCO_2eq\ MWh^{-1}$) and close to the mean (55 $kgCO_2eq\ MWh^{-1}$) found in a recent review on Li-ion battery energy storage systems [40]. Noteworthy, this review discussed that variability in embodied emissions is more dependent on the source of data than on the type of Li-ion battery technology, indicating a substantial level of uncertainty in determining the battery system impacts.

Like electrochemical batteries, hydro reservoirs are associated with significant life cycle impacts (direct land use change, dam construction, methane emissions, among others) [41]. This impact appears as a relatively high emission factor of hydropower (71.7 $kgCO_2e\ MWh^{-1}$) when calculating the grid mean emission factor (**Table S9**). Moreover, the use of water resources must be framed within a context of resilience and adaptation to climate change, where hydropower generation may be adversely impacted by decreased precipitation and increased temperatures [42–44]. Therefore, efficient utilization of energy storage is vital for the economic and carbon efficiencies of e-H_2 production.

This work assumes that e-H_2 production can use the existing energy reservoirs of the grid without allocation of impacts. The feasibility of energy storage without net addition of impacts can only be justified if the new usage does not stress the hydropower capacity and the hydro reservoirs. In other words, conditions must be established to ensure that e-H_2 production preserves the hydropower functionality available for the other generators and consumers connected to the grid.

3.4. Metrics of hydropower stress

Three metrics of hydropower stress calculated within a week are illustrated in Fig. 4A: (i) minimum and (ii) maximum generation (in units of GW) and (*iii*) maximum power ramp (in units of GW h^{-1}). The minimum is associated with a risk of energy curtailment (water spilling) because minimum streamflow must be kept in the river basins. The maximum is associated with a risk of fossil dispatch (and induced GHG emissions) to meet the peak loads. The hydropower ramp is the primary source of fast-response power capacity within the grid, thus a critical asset for grid flexibility.

The simulated scenarios of e-H_2 production (Table 1) modify hydro generation to account for the differences between solar or wind power generation and consumption in e-H_2 production (Eq. 3). Scenarios S100 and W100 consider a constant consumption of 1 GW. Scenario S30 uses a designed consumption profile that closely (but not exactly) matches the solar generation (Fig. 4B). Scenario W90 uses a designed consumption profile that turns off the electrolyzer at peak demand hours on low-wind days (Fig. 4C). The selected week shown in Fig. 4A–C is in March, when solar generation is close to the annual mean, while wind generation is below it (Fig. 3E). For comparison, a week in October (when wind power is above the mean) is presented in **Fig. S5** with data from the S30, S100, W90, and W100 scenarios.

The changes in the hydropower stress parameters for the e-H_2 production scenarios are shown in Fig. 4D–I. The data points are calculated for each week (Fig. 4D-F), with the x-axes reflecting the variability observed in the SIN operation (base case) and the y-axes presenting the changes induced by the additional e-H_2 production (scenarios S100, S30, W100, and W90). The boxplots present a statistical view of the induced changes across the entire year (Fig. 4G–I). The results of the alternative simulations with 5 GW of electrolyzer capacity are presented in Fig. S6. The S100 scenario adds stress to the three hydropower

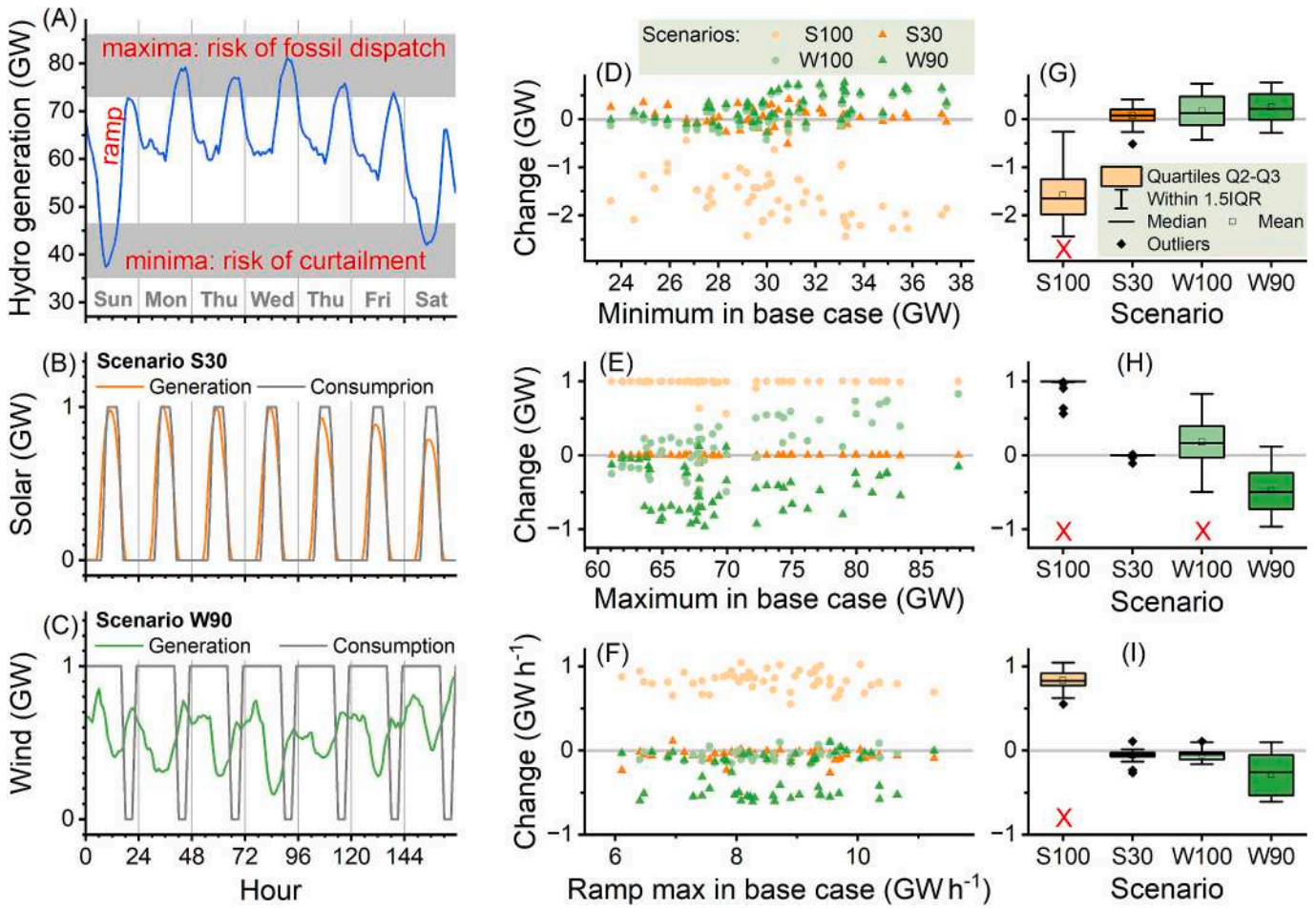

Fig. 4. Metrics of hydropower stress in the simulated e-H_2 production scenarios. An exemplary week (sunday 03/17/2024 to saturday 03/23/2024) illustrates (A) hydro generation in the base case with indicators of stress (minima, maxima, and ramp); (B) solar energy generation and consumption in scenario S30 and (C) wind energy generation and consumption in scenario W90. (D—F) Changes in hydropower stress metrics (D: minimum, E: maximum, and F: ramp maximum) versus observations in the base case. The changes are promoted by the additional e-H_2 production and are calculated for each calendar week within the simulated year (04/30/2023 to 04/29/2024). (G–I) Boxplots of the changes in (D—F). The red crosses mark the cases with a tendency to increase the maxima or decrease the minima, which would be stressors of hydropower flexibility and thus disqualified under the criteria of hydro utilization without net addition of impacts. (For interpretation of the references to color in this figure legend, the reader is referred to the web version of this article.)

parameters. The maxima are increased, the minima are decreased, and the ramps are accentuated. This result reflects that solar power is already a stressor of hydropower flexibility in the base-case scenario, and the added solar capacity to meet e-H_2 production aggravates the stress.

In contrast, the wind W100 scenario consistently adds stress only by increasing the hydropower maxima (Fig. 4H), while the response of minima (Fig. 4G) and ramp maxima (Fig. 4I) tends to de-stress the hydropower. The better performance of wind (W100) compared to solar (S100) can be attributed to the daily profile of wind with smoother variations and complementarity to solar (Fig. 3F). Nevertheless, the degradation of at least one stress metric would not qualify the S100 and W100 scenarios for the assumed utilization of the hydro capacity without the net addition of impacts.

Energy consumption profiles in the S30 and W90 scenarios were designed not to stress the hydropower metrics. Judging by the positions of the median, mean, or interquartile ranges, the boxplots of Fig. 4G–I show that these design criteria were accomplished. Therefore, the S30 and W90 scenarios would qualify as users of the legacy of hydropower without net addition of impacts. These scenarios offer significant extensions of the electrolyzer CF compared to an hourly matching requirement. Solar capacity factors between 16.2 and 24.9 % (Fig. 2A) or 24 % (mean from ONS data) were extended to an e-H_2 production with CF = 30 % in the S30 scenario. Further extension of solar e-H_2 capacity factors would require dedicated (behind the meter) energy storage, which is beyond the scope of this work (Fig. 1) but has been examined as an attractive option in different contexts [1,5].

For wind energy, capacity factors of up to 45 % (Fig. 2) or 41 % (mean from ONS data) are extended to CF = 90 % in the W90 scenario of e-H_2 production. Such extensions of e-H_2 output are achieved without dedicated energy storage (Fig. 1) nor net impacts on the hydro stress parameters (Fig. 4), demonstrating the potential for enhanced systemic efficiency of the designed W90 energy consumption profiles.

3.5. *Impacts on the annual cycle of hydro reservoirs*

For the simulated e-H_2 scenarios, the mismatches between the additional energy generation and consumption were met by the legacy hydropower (Eq. 3). While the previous section examined the impacts on the weekly profiles of power, this section analyzes the impacts on the annual cycle of energy storage in the hydro reservoirs. Energy storage in the base case scenario (Fig. 5A) shows the typical cycle of energy storage in the SIN due to the seasonality of the streamflow energy (Fig. 3E) combined with the dominance of hydro generation (Fig. 3C). Hydro reservoirs reach a maximum by the transition from wet to dry season (around April–June) and, conversely, reach a minimum by the transition

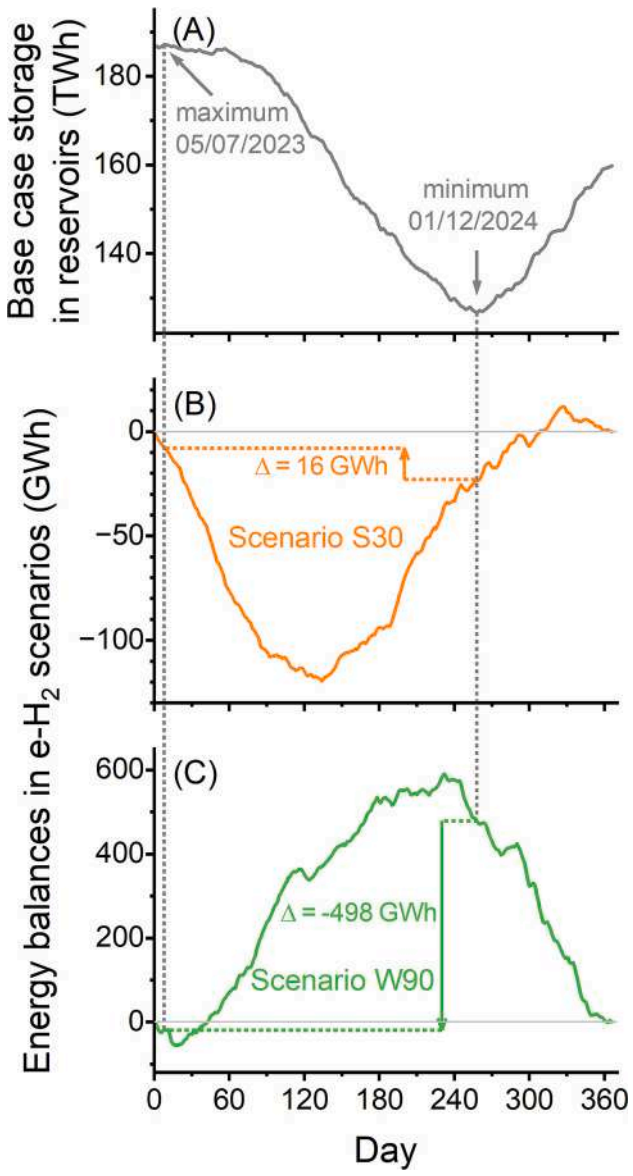

Fig. 5. Energy balances through the simulated year (04/30/2023 to 04/29/2024). (A) Base case energy storage in hydro reservoirs observed in the SIN. (B, C) energy balances in the S30 (B) and W90 (C) scenarios of e-H_2 production. The induced impacts Δ on the utilization of energy storage in hydro reservoirs are indicated.

from dry to wet season (around November–January). During the simulation year (04/30/2023–04/29/2024), the maximum is observed by 05/07/2023 and the minimum by 01/12/2024. The reservoirs did not fully recover in the analyzed year due to relatively low rainfall. Nevertheless, our analysis is dedicated to how grid-based energy storage is changed as a consequence of the e-H_2 scenarios, focusing on the changes in energy demand from the reservoirs.

The energy balances of the S30 and W90 scenarios (Figs. 5B–C) end up equal to zero due to the modeled condition of annual matching (Eq. 4). However, the energy balances fluctuate at positive and negative domains, reflecting the seasonality of the solar and wind resources (Fig. 3E). The induced impact on reservoir utilization is slightly positive (Δ = 16 GWh) for the S30 scenario, indicating that this solar scenario would be a stressor of the annual cycle of the reservoirs. Adjusting the S30 consumption profiles to operate longer hours in summer and shorter hours in winter would be needed to solve this stress in the reservoirs while keeping an electrolyzer CF = 30 %. Noteworthy, the magnitude of the stress in the reservoirs (Δ = 16 GWh) corresponds to only 0.6 % of the energy (2635 GWh) generated and consumed by the S30 scenario during the simulated year.

On the other hand, for the W90 scenario, the induced impact on reservoir utilization is strongly negative (Δ = −498 GWh), implying that wind-powered e-H_2 production would reduce the demand for grid-based energy storage in the annual cycle. This result arises from the seasonal profile of wind (Fig. 3E), which complements the legacy of hydro that dominates the grid's renewable capacity (Fig. 3D).

The result that wind power with a capacity factor of 41 % (mean of SIN from ONS data) can back e-H_2 production with CF = 90 % (W90 scenario) without detrimental impacts on the grid is remarkable and should be appreciated thoughtfully. This systemic efficiency is enabled by the wind seasonal complementarity with hydro (Fig. 3E) and daily complementarity with solar (Fig. 3F), combined with installed capacities lower for wind than for hydro and solar (Fig. 3D). A comparison with studies performed in other contexts helps to highlight the importance of this result. Terlouw et al. modeled cost-optimal autonomous e-H_2 systems in European islands with solar and wind energy sources aided by battery storage. Their model obtained CF = 48–64 %, exemplifying CF limits without a grid connection [5]. Zeyen modeled grid-connected e-H_2 systems in continental Europe. Their models requiring hourly matching reached CF ~ 40–60 % unless substantial battery storage was added to enable CF = 100 % [9]. Ricks et al. modeled grid-connected e-H_2 in the United States Western Interconnection system, including the effects of subsidies for e-H_2 production. In their model, under an hourly time-matching requirement, a high CF = 71–99 % was reached through procuring an overcapacity of solar and wind energy. However, several grid zones showed substantial consequential emissions (up to ~35 $kgCO_2eq\ kgH_2^{-1}$), exemplifying how the high CF might be associated with indirect emissions from grid-connected fossil power sources. Against this background of limitations on CF, the W90 scenario of this work solves such constraints by harnessing synergies with the legacy of renewables in the SIN, without adding renewable overcapacity nor increasing grid emissions due to fossil dispatch.

3.6. Carbon intensities of grid-connected e-H_2

After demonstrating the possibility of utilizing the legacy of hydropower and hydro reservoirs without net addition of impacts, this section consolidates the e-H_2 carbon intensities accounting for the energy source, transmission, and e-H_2 production. The first case presented in Table 2 and Fig. 6 is e-H_2 production with CF = 90 % using the grid mix of power sources (i.e., not explicitly using additional solar or wind energy). This grid-mix case presents an emission factor of 85.2 $kgCO_2eq\ MWh^{-1}$ (Table S9) and a carbon intensity of 5.9 $kgCO_2eq\ kgH_2^{-1}$. This case would not qualify as low-carbon e-H_2 in many jurisdictions [45] because it brings only a ≈ 50 % reduction in emissions compared to H_2 obtained from steam reforming of natural gas (11.4 $kgCO_2eq\ kgH_2^{-1}$) [20,21]. The share of fossil energy and the relatively high emission factor of hydropower (**Table S9**) are responsible for the high carbon budget despite the 93 % share of renewables in the grid. This result demonstrates the need to back the e-H_2 production with low-carbon energy, even in a highly decarbonized grid.

Wind energy leads to the lowest e-H_2 carbon intensities, from 1.0 to 2.7 $kgCO_2eq\ kgH_2^{-1}$ (Fig. 6). The wind scenarios assume electrolysis with CF = 90 %, consistent with the simulated scenario W90 (Table 1). Long-distance (2000 km) electricity transmission adds 0.1–0.4 $kgCO_2eq\ kgH_2^{-1}$, much less than the 1.5–1.6 $kgCO_2eq\ kgH_2^{-1}$ that is added by moving from the best (7.9 $kgCO_2eq\ MWh^{-1}$) to ordinary (31.3 $kgCO_2eq\ MWh^{-1}$) wind energy emission factors. This result shows that energy sourcing from the best wind sites is critical to reaching the lowest carbon intensities. Moreover, the footprint of long-distance transmission is small enough to produce low-carbon e-H_2 in the SE-CO subsystem, with energy sourcing from wind sites primarily located in the N, NE, and S subsystems (see Fig. 2 and Fig. 3A). This result indicates that the entire

Table 2
Contributions to the e-H_2 carbon intensities in the distinct pathways for grid-connected e-H_2 production.

Energy source	Electrolyzer CF (%)	Transmission scenario	Emission factor of energy source ($kgCO_2eq\ MWh^{-1}$)	Energy consumption ($kWh\ kgH_2^{-1}$) [a]	Energy impact ($kgCO_2eq\ kgH_2^{-1}$)	Transmission infrastructure ($kgCO_2eq\ kgH_2^{-1}$)	Electrolyzer and Balance of Plant (BoP) ($kgCO_2eq\ kgH_2^{-1}$)
grid	90	Grid mean	85.2	64.6	5.50	0.18	0.26
solar	30	Grid mean	31.3	64.6	2.02	0.18	0.69
			48.0	64.6	3.10	0.18	0.69
		Grid mean + 2000 km HVDC	31.3	68.0	2.13	0.44	0.69
			48.0	68.0	3.26	0.44	0.69
wind	90	Grid mean	7.9	64.6	0.51	0.18	0.26
			31.3	64.6	2.02	0.18	0.26
		Grid mean + 2000 km HVDC	7.9	68.0	0.54	0.27	0.26
			31.3	68.0	2.13	0.27	0.26

Unit conversions: 1 $kgCO_2eq\ MWh^{-1}$ = 0.28 $gCO_2eq\ MJ^{-1}$; 1 $kgCO_2eq\ kgH_2^{-1}$ = 8.33 $gCO_2eq\ MJ^{-1}$.
[a] Include transmission losses.

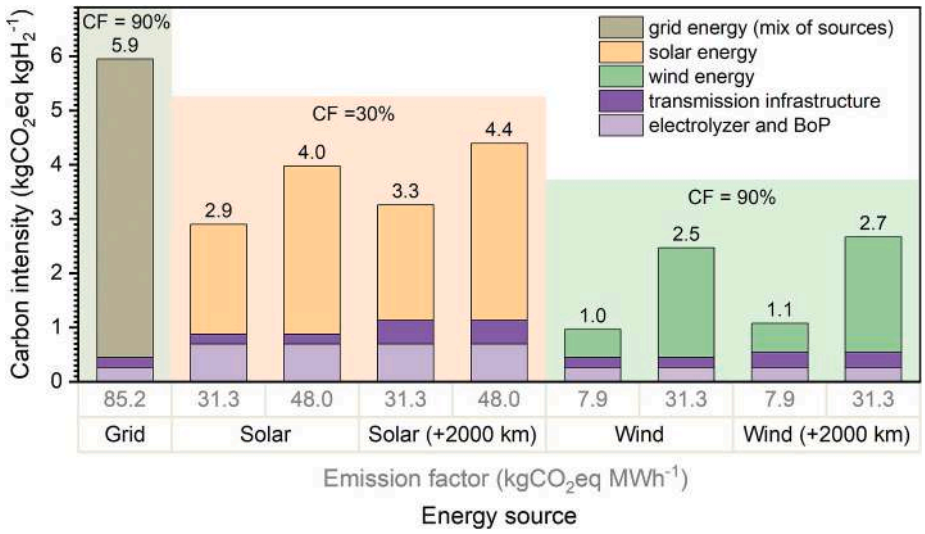

Fig. 6. Carbon intensity of distinct pathways for grid-connected e-H_2 production. CF: Electrolysis capacity factor. Unit conversions: 1 $kgCO_2eq\ MWh^{-1}$ = 0.28 $gCO_2eq\ MJ^{-1}$; 1 $kgCO_2eq\ kgH_2^{-1}$ = 8.33 $gCO_2eq\ MJ^{-1}$.

grid can benefit from low-carbon wind energy if electricity transmission is unconstrained. Therefore, wind-powered e-H_2 can be produced at the sites of H_2 utilization, such as steel, fuels, and chemicals industrial sites [3,4].

Solar energy has carbon emission factors ($kgCO_2eq\ MWh^{-1}$) higher than wind energy (Fig. 2), and its temporal profile limits the e-H_2 capacity factor, as shown by the W30 scenario (Table 1). These characteristics resulted in higher carbon intensities of solar-backed e-H_2 (Table 2 and Fig. 6). The lowest carbon intensity (2.9 $kgCO_2eq\ kgH_2^{-1}$) is achieved by energy sourcing from the best solar sites and positioning the e-H_2 production nearby (e.g., within the same SIN subsystem). On the contrary, the highest carbon intensity (4.4 $kgCO_2eq\ kgH_2^{-1}$) corresponds to energy sourcing from the worst solar sites coupled with long-distance electricity transmission. This worst-case scenario is unrealistic because sourcing from inferior solar sites and electricity transmission to superior sites cannot be justified. In the analysis of this work, the reduced e-H_2 capacity factor (CF = 30 %) with solar energy also penalizes the carbon intensity attributed to the long-distance transmission infrastructure and the e-H_2 production system (electrolyzer and BoP) (Fig. 6). These penalties further degrade the performance of solar compared to wind.

Electrolysis itself dominates the impact of the electrolysis system. Energy consumption for electrolysis (60.3 kWh kgH_2^{-1}) is much greater than for desalination (0.04 kWh kgH_2^{-1}) and compression (0.65 kWh kgH_2^{-1}). Moreover, for the CF = 90 % scenarios (Table 2 and Fig. 6), the electrolyzer and BoP carbon footprint was calculated at 0.26 $kgCO_2eq\ kgH_2^{-1}$, with the major contribution coming from the electrolyzer stack (71 %) compared to desalination (11 %), H_2 compression (7 %), and other BoP components (11 %). This electrolyzer footprint is within the range (0.14–0.28 $kgCO_2eq\ kgH_2^{-1}$) reported by Krishnan et al., who made an independent analysis and compiled several studies of alkaline electrolysis systems [46]. The lifetime of the alkaline electrolyzer and its impact on emissions accounting is a significant uncertainty of the present work. A penalized electrolyzer footprint of 0.69 $kgCO_2eq\ kgH_2^{-1}$ was calculated for the solar-backed CF = 30 % scenarios (Table 2 and Fig. 6). The higher footprint compared to the CF = 90 % scenarios arises from the reduced e-H_2 production during the electrolyzer and BoP service life. Although uncertain, this assumption exemplifies that the electrolyzer footprint may become significant if the e-H_2 output is degraded within the service life. Noteworthy, the designed temporal profiles S30 and W90 (Fig. 4B-C) offer predictability and consistency to the electrolyzer operation, which may help enhance the electrolyzer's longevity [47–50]. Such beneficial impacts on electrolyzer operability may be an additional source of economic and carbon efficiency enabled by harnessing the network effects between the additional e-H_2 and the legacy of renewable assets in the grid. It is worth mentioning that the sensitivity analysis (**Figs. S1–3**) shows that the energy source is the most influential factor in determining the e-H_2 carbon intensity, while all scenarios benefit from improvements in equipment performance and longevity.

For a final comparison, it is worth noting that most e-H_2 regulation

studies generally focus on the emissions from energy generation (Scope 2 from GHG Protocol), which lead to e-H_2 carbon intensities equal to zero for energy supplied by solar or wind. On the other hand, the life cycle assessment integrates the embodied emissions associated with creating the infrastructure for energy generation, transmission, and consumption in the electrolysis plant (Fig. 6). As de Kleijne et al. recently noted, the broader life cycle perspective raises concerns that regulations not accounting for component manufacturing and H_2 leakage will offer an unrealistic picture of the e-H_2 carbon footprint [51].

Moreover, several authors recently calculated independently the life cycle carbon intensities of solar- and wind-powered e-H_2. Despite differences in methodologies, assessed technologies, and local conditions, the values are consistent with those obtained in the present work. For example, de Kleijne et al. analyzed the case of the European Union and reported 1.7–4.4 $kgCO_2eq\ kgH_2^{-1}$ for solar and 0.4–0.8 $kgCO_2eq\ kgH_2^{-1}$ for offshore wind energy [6]. Garcia and Oliva analyzed Chile's case and reported 2.0–7.1 $kgCO_2eq\ kgH_2^{-1}$ for solar and 0.85–2.21 $kgCO_2eq\ kgH_2^{-1}$ for wind [52]. Patel et al. compared several pathways of H_2 production, reporting 2.5 $kgCO_2eq\ kgH_2^{-1}$ for e-H_2 from solar and 0.6 $kgCO_2eq\ kgH_2^{-1}$ from wind energy [53].

4. Discussion

4.1. Reframing the requirements for low-carbon e-H_2

As argued alongside the presentation of the results, the carbon footprints calculated in this work were consistent with previous studies dedicated to distinct local conditions. This consistency was observed for the carbon emission factors of solar and wind energy (**section 3.1**) and the e-H_2 carbon intensities (**section 3.6**). The carbon footprints are primarily influenced by the types, efficiencies, and lifetimes of the employed technologies, which explains why the footprints show relatively narrow ranges of variations across distinct geographies. On the other hand, the electricity sourcing requirements for grid-connected e-H_2 aim to ensure that the additional e-H_2 production does not induce detrimental impacts on the grid. Therefore, the grid characteristics influence the requirements, which must be carefully examined. The analyzed case study of a large-scale decarbonized grid thus allows one to reframe the additionality, deliverability, and temporality requirements to ensure the carbon integrity of grid-connected e-H_2.

As for additionality, the dominance of renewable energy in the grid legacy (Fig. 3C) and expansion (Fig. 3D) indicates that this requirement has an open avenue to be met. A significant concern with the practical implementation of additionality is its reliance on economic models to determine whether contractual instruments (power purchase agreements and energy attribute certificates) warrant that a renewable energy source is genuinely additional compared to a counterfactual baseline without e-H_2 production [7,54]. Reliance on models has been a source of lengthy controversy in other areas of sustainability research, notably in modeling biofuel's indirect land-use change (iLUC) [55]. In the context of iLUC, recommendations towards common criteria for sustainable fuels have recognized modeling limitations and advised adopting risk-based approaches in the near term and enforcing land-use regulations in the long term [45]. An analogy with the e-H_2 additionality requirement is proposed here. For a grid dominated by renewables, the analysis of additionality may adopt a qualitative risk-based approach in the short term until the grids become fully decarbonized in the long term. For instance, a risk-based approach may emphasize a verifiable contribution of e-H_2 to the phase-out of fossil energy sources. Such an approach is possible because fossil dispatch is the operator's response to stress factors, notably hydropower restrictions in years of drought and peak power demand after sunset (Fig. 3E). As exemplified by the decline of peak demand in the W90 scenario (Fig. 4H), a flexible e-H_2 operation to attenuate grid stress can contribute to the phase-out of fossil energy sources. Noteworthy, grid stress and the consequent need for fossil dispatch correlate with higher energy spot prices, opening the way for price-based decoupling of fossil energy and e-H_2 production.

As for deliverability, this work demonstrated that electricity transmission can connect the points of energy generation and consumption within the SIN with emissions associated with transmission infrastructure ($<0.5\ kgCO_2eq\ kgH_2^{-1}$) that do not compromise the low-carbon credentials of e-H_2 (Table 2). The deliverability requirement is thus reduced to the availability of transmission capacity, lifting restrictions associated with long distances. Current transmission capacity ensures strong integration of the SIN subsystems. For example, during the simulated year, the transmission between the NE and SE-CO subsystems reached ~12 GW (ONS data, **Table S8**), a significant share of the ~80 GW of the entire SIN generation (Fig. 3F). The integration is also favored by the energy storage distributed within the SIN (Fig. 3C), which is operated to equalize energy prices (**Fig. S4**). These facts demonstrate that the distinction of subsystems per se is not a sound restriction for a deliverability requirement, and the degree of integration between the subsystems must be considered.

The most significant reframing needs to be directed to the temporal requirement. First, the wording of temporal "matching" is misleading because there are types of temporal unmatching that are beneficial to the grid and should be permissible. The requirement is thus more broadly rephrased as "temporality." The diversity of renewable power sources distributed on a continental scale and the substantial energy storage in hydro reservoirs directed attention to the temporal complementarity among the renewable sources and the possibility of changing the reservoir's operation without net addition of impacts. Therefore, this case study demonstrated that hourly matching is an unsound requirement. It tentatively isolates the e-H_2 production elements from the grid's system-level opportunities for synergistic addition of grid-connected e-H_2.

4.2. Regulation of e-H_2 in the Brazilian grid

The Brazilian low-carbon hydrogen policy became law by August 2024 [56]. The law established that low-carbon H_2 will be certified, and life cycle assessment will determine its carbon intensity. The limit of 7 $kgCO_2eq\ kgH_2^{-1}$ defines what qualifies as "low-carbon" under the law. This threshold is higher than most definitions in other jurisdictions [45]. It would qualify as low-carbon the e-H_2 obtained from the grid average emission factor of 2023 (5.9 $kgCO_2eq\ kgH_2^{-1}$, see Table 2 and Fig. 6). The law does not explicitly mention additionality; regulatory executive acts are yet pending. It is currently unclear how the characteristics of the Brazilian grid will be translated into the regulatory and certification frameworks. Nevertheless, it is clear from this study that methodological innovation is needed. This need may position the Brazilian case as a benchmark for e-H_2 methodologies in contexts of large-scale grids dominated by renewables.

4.3. Universalizing a novel temporality requirement

The hourly matching requirement has been incorporated into the language of e-H_2 research literature, regulations, and certification methodologies. Among the several criticisms made to hourly matching, the analysis by Zeyen et al. of selected European regions is highlighted here. It concluded that low-emissions and low-cost e-H_2 production could also be reached with annual or monthly matching if further requirements are set to limit the electrolyzer CF or limit the price of electrical energy used for e-H_2 production or if the grid already has a high share of renewables and coal is phased out [9]. Based on the lessons from the present Brazilian case study, which further demonstrated the inadequacy of hourly matching, this section discusses the fundamentals of a novel temporality requirement that could eventually apply to any grid.

The temporality requirement proposed here defines the permissible temporal unmatching between the additional energy generation and

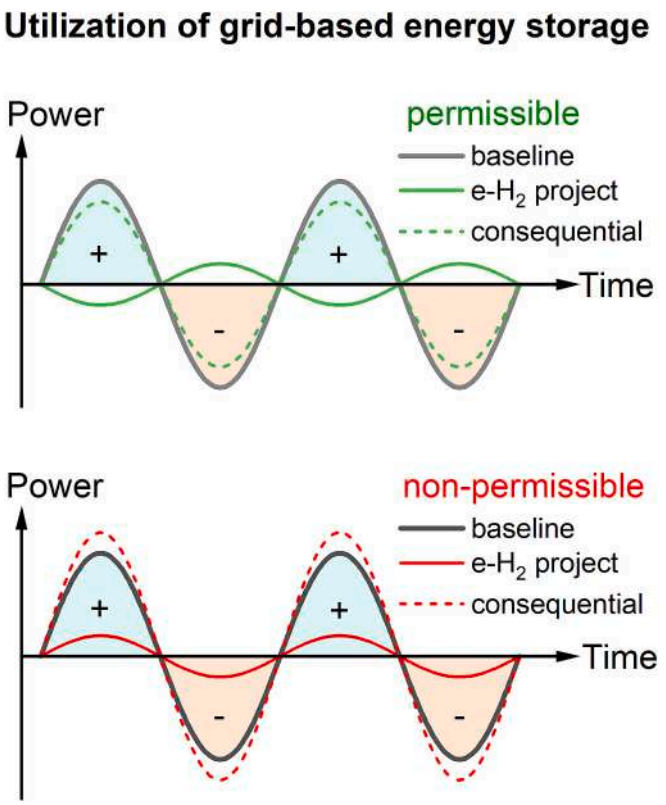

Fig. 7. Schematic representation of charge (+) and discharge (−) cycles of grid-based energy storage. Adding an e-H_2 project can either decrease (top) or increase (bottom) the demand for grid-based storage, depending on the temporal correlations between the e-H_2 project and the grid baseline. The cases would be permissible (top) or non-permissible (bottom) under a requirement of no consequential expansion of grid-based storage. The permissible case needs a renewable power source presenting temporal complementarity with the legacy of renewables.

consumption for e-H_2 production. The permissible temporal unmatching generates a demand for energy storage that promotes no consequential expansion of grid-based storage. Fig. 7 illustrates permissible and non-permissible cases. The key to the permissible case is the temporal complementarity between the grid baseline and the e-H_2 addition. The two key ingredients of this temporality requirement are grid-based energy storage and the opportunity to add complementary renewable capacity. Both ingredients tend to become more prominent as grids decarbonize, and recognition of this effect will promote complementarity.

Temporal complementarities among renewable resources are ubiquitous in analyzing large-scale renewable energy systems. Solar-wind complementarity is observed in many world regions, as informed by a recent review article [57] and a dedicated atlas [58]. In such areas, a grid with a legacy dominated by solar would favor an expansion of wind and vice versa. The determination of permissible temporal unmatching would capture such preferences. In addition, cross-regional complementarities become increasingly crucial as the grids grow in spatial coverage. The hydro-wind coupling within the SIN is an example of cross-regional complementarity (Fig. 3C–E). Solar-solar complementarity tends to be negligible due to the shared solar cycles in the daily and annual time scales. On the other hand, wind-wind spatial complementarity may be significant, as revealed by an analysis of wind profiles across China [59]. Based on the ubiquity of temporal complementarities, this study is expected to stimulate analyses of other grids to quantify the permissible temporal unmatching and guide e-H_2 methodologies beyond the unsound restrictions imposed by hourly matching.

5. Conclusions

This work examined the carbon intensity and the requirements to ensure the carbon integrity of grid-connected e-H_2 production. The life cycle assessment determined e-H_2 carbon intensities ($kgCO_2eq\ kgH_2^{-1}$) accounting for the embodied emissions of energy generation (solar and wind), transmission, and the electrolysis plant. A unique perspective was achieved by investigating e-H_2 in the Brazilian National Interconnected System, a large-scale grid that is highly decarbonized, extended on a continental scale, and served by substantial energy storage. By uniting a cradle-to-gate life cycle assessment and an analysis of induced impacts on the grid, the study established a comprehensive evaluation of low-carbon e-H_2 production in Brazil.

Furthermore, the study tested whether the electricity sourcing requirements formulated to ensure the carbon integrity of e-H_2 could be applied to a large-scale decarbonized grid. The analysis revealed that the requirements of additionality, deliverability, and temporality should be reframed, with immediate implications for e-H_2 regulation and certification methodologies applicable to large-scale grids rich in renewables. Additionality has an open avenue to be met in a grid dominated by renewables; risk-based approaches may be considered as substitutes for contractual instruments to ensure that renewable capacity is added to supply e-H_2 production. As for deliverability, it should focus on the existence of transmission capacity, not on distances between energy generation and consumption, because the impacts of long-distance (up to $\sim 10^3$ km) transmission do not compromise the low-carbon credentials of e-H_2. Lastly, temporality should recognize the existence of types of temporal unmatching between energy generation and consumption that do not add net impacts to the grid and thus should be permissible. Permissible temporal unmatching emerges from the existing grid-based energy storage and the temporal complementarities between the legacy and the additional renewable power sources.

CRediT authorship contribution statement

Carlos E. Driemeier: Writing – review & editing, Writing – original draft, Validation, Methodology, Funding acquisition, Formal analysis, Conceptualization. **Giovana C. Tonon:** Writing – review & editing, Writing – original draft, Visualization, Methodology, Formal analysis, Data curation. **Mateus F. Chagas:** Writing – review & editing, Supervision, Methodology, Investigation, Formal analysis, Data curation, Conceptualization. **Gabriel P. Petrielli:** Writing – review & editing, Visualization, Methodology, Formal analysis, Data curation. **Daniele S. Henzler:** Writing – review & editing, Investigation, Formal analysis. **Luísa C.M. Gomes:** Writing – review & editing, Investigation, Formal analysis. **Bruno E. Limeira:** Writing – review & editing, Validation, Conceptualization. **Thayse A.D. Hernandes:** Writing – review & editing, Supervision, Resources, Conceptualization. **Edvaldo R. Morais:** Writing – review & editing, Supervision, Resources, Conceptualization.

Funding sources

This research was funded by the Brazilian Ministry for Science, Technology, and Innovations (MCTI) and the National Council for Scientific and Technological Development (CNPq grant 408016/2024–8).

Declaration of competing interest

The authors declare that they have no known competing financial interests or personal relationships that could have appeared to influence the work reported in this paper.

Appendix A. Supplementary data

Supplementary data to this article can be found online at https://doi.org/10.1016/j.apenergy.2025.125938.

Data availability

The analysis of the electricity grid was carried out using publicly available data from the ONS. Additional data supporting this article have been included in the Supplementary Material.

References

[1] Mallapragada DS, Gençer E, Insinger P, Keith DW, O'Sullivan FM. Can industrial-scale solar hydrogen supplied from commodity technologies be cost competitive by 2030? Cell Rep Phys Sci 2020;1:100174. https://doi.org/10.1016/j.xcrp.2020.100174.

[2] IRENA. Green hydrogen cost reduction: scaling up electrolysers to meet the 1.5^0 C climate goal. 2020.

[3] Azadnia AH, McDaid C, Andwari AM, Hosseini SE. Green hydrogen supply chain risk analysis: a european hard-to-abate sectors perspective. Renew Sust Energ Rev 2023;182:113371. https://doi.org/10.1016/j.rser.2023.113371.

[4] Superchi F, Mati A, Carcasci C, Bianchini A. Techno-economic analysis of wind-powered green hydrogen production to facilitate the decarbonization of hard-to-abate sectors: a case study on steelmaking. Appl Energy 2023;342:121198. https://doi.org/10.1016/j.apenergy.2023.121198.

[5] Terlouw T, Bauer C, McKenna R, Mazzotti M. Large-scale hydrogen production *via* water electrolysis: a techno-economic and environmental assessment. Energy Environ Sci 2022;15:3583–602. https://doi.org/10.1039/D2EE01023B.

[6] de Kleijne K, de Coninck H, van Zelm R, Huijbregts MAJ, Hanssen SV. The many greenhouse gas footprints of green hydrogen. Sustain Energy Fuels 2022;6:4383–7. https://doi.org/10.1039/D2SE00444E.

[7] Giovanniello MA, Cybulsky AN, Schittekatte T, Mallapragada DS. The influence of additionality and time-matching requirements on the emissions from grid-connected hydrogen production. Nat Energy 2024;9:197–207. https://doi.org/10.1038/s41560-023-01435-0.

[8] Ricks W, Xu Q, Jenkins JD. Minimizing emissions from grid-based hydrogen production in the United States. Environ Res Lett 2023;18:014025. https://doi.org/10.1088/1748-9326/acacb5.

[9] Zeyen E, Riepin I, Brown T. Temporal regulation of renewable supply for electrolytic hydrogen. Environ Res Lett 2024;19:024034. https://doi.org/10.1088/1748-9326/ad2239.

[10] Union European. Commission delegated regulation (EU) 2023/1184. European Union; 2023.

[11] Department of the Treasury. Section 45V credit for production of clean hydrogen. United States. 2023.

[12] Brandt J, Iversen T, Eckert C, Peterssen F, Bensmann B, Bensmann A, et al. Cost and competitiveness of green hydrogen and the effects of the European Union regulatory framework. Nat Energy 2024;9:703–13. https://doi.org/10.1038/s41560-024-01511-z.

[13] Ruhnau O, Schiele J. Flexible green hydrogen: the effect of relaxing simultaneity requirements on project design, economics, and power sector emissions. Energy Policy 2023;182:113763. https://doi.org/10.1016/j.enpol.2023.113763.

[14] Tolmasquim MT, de Barros Correia T, Addas Porto N, Kruger W. Electricity market design and renewable energy auctions: the case of Brazil. Energy Policy 2021;158:112558. https://doi.org/10.1016/j.enpol.2021.112558.

[15] ONS. Operador Nacional do Sistema. ONS. https://www.ons.org.br/; 2024 [accessed June 19, 2024].

[16] EPE. BEN summary report: Reference year 2023. Rio de Janeiro. 2024.

[17] BloomberNEF. 'Green' Hydrogen to Outcompete 'Blue' Everywhere by 2030. 2021. https://about.bnef.com/blog/green-hydrogen-to-outcompete-blue-everywhere-by-2030/.

[18] Botelho DF, Moraes CA, de Oliveira LW. Green hydrogen production from hydro spilled energy in Brazilian hydropower plants. Int J Hydrog Energy 2024;68:575–85. https://doi.org/10.1016/j.ijhydene.2024.04.255.

[19] Pinheiro FP, Gomes DM, Tofoli FL, Sampaio RF, Melo LS, Gregory RCF, et al. Techno-economic analysis of green hydrogen generation from combined wind and photovoltaic systems based on hourly temporal correlation. Int J Hydrog Energy 2025;97:690–707. https://doi.org/10.1016/j.ijhydene.2024.11.429.

[20] Wernet G, Bauer C, Steubing B, Reinhard J, Moreno-Ruiz E, Weidema B. The ecoinvent database version 3 (part I): overview and methodology. Int J Life Cycle Assess 2016;21:1218–30. https://doi.org/10.1007/s11367-016-1087-8.

[21] Ecoinvent. Ecoinvent database. 2023.

[22] Wei W, Li J, Chen B, Wang M, Zhang P, Guan D, et al. Embodied greenhouse gas emissions from building China's large-scale power transmission infrastructure. Nat Sustain 2021;4:739–47. https://doi.org/10.1038/s41893-021-00704-8.

[23] Miyakawa H, Maghram Al Shaiae M, Green TN, Ito Y, Sugawara Y, Onishi M, et al. Reliable Sea water Ro operation with high water recovery and no-chlorine/no-Sbs dosing in Arabian gulf, Saudi Arabia. Membranes (Basel) 2021;11:141. https://doi.org/10.3390/membranes11020141.

[24] Gerloff N. Comparative life-cycle-assessment analysis of three major water electrolysis technologies while applying various energy scenarios for a greener hydrogen production. J Energy Storage 2021;43:102759. https://doi.org/10.1016/j.est.2021.102759.

[25] Veiga SF, Nobre P, Giarolla E, Capistrano V, Baptista M, Marquez AL, et al. The Brazilian earth system Model Ocean-atmosphere (BESM-OA) version 2.5: evaluation of its CMIP5 historical simulation. Geosci Model Dev 2019;12:1613–42. https://doi.org/10.5194/gmd-12-1613-2019.

[26] Xavier AC, Scanlon BR, King CW, Alves AI. New improved Brazilian daily weather gridded data (1961–2020). Int J Climatol 2022;42:8390–404. https://doi.org/10.1002/joc.7731.

[27] Ma T, Yang H, Lu L. Solar photovoltaic system modeling and performance prediction. Renew Sust Energ Rev 2014;36:304–15. https://doi.org/10.1016/j.rser.2014.04.057.

[28] Pan L, Shao C. Wind energy conversion systems analysis of PMSG on offshore wind turbine using improved SMC and extended state observer. Renew Energy 2020;161:149–61. https://doi.org/10.1016/j.renene.2020.06.057.

[29] Pereira E, Martins F, Gonçalves A, Costa R, Lima F, Rüther R, et al. Atlas brasileiro de energia solar. Universidade Federal de São Paulo; 2017. https://doi.org/10.34024/978851700089.

[30] Neiva AC, De B, Dutra RM, de SRFC Mello, Guedes VG, AAM Cabrera, et al. Atlas do Potencial Eólico Brasileiro - Simulações 2013. Rio de Janeiro: CEPEL; 2017.

[31] The World Bank Group. Global Solar Atlas. https://globalsolaratlas.info/map; 2024. accessed August 31, 2024.

[32] Davis NN, Badger J, Hahmann AN, Hansen BO, Mortensen NG, Kelly M, et al. The global wind atlas: a high-resolution dataset of Climatologies and associated web-based application. Bull Am Meteorol Soc 2023;104:E1507–25. https://doi.org/10.1175/BAMS-D-21-0075.1.

[33] Tawalbeh M, Al-Othman A, Kafiah F, Abdelsalam E, Almomani F, Alkasrawi M. Environmental impacts of solar photovoltaic systems: a critical review of recent progress and future outlook. Sci Total Environ 2021:759. https://doi.org/10.1016/j.scitotenv.2020.143528.

[34] IEA. Life cycle upstream emission factors 2023 (Pilot Edition) Database documentation. Paris. 2023.

[35] NREL. Life cycle greenhouse gas emissions from electricity generation: Update. Golden. 2021.

[36] Ávila L, Mine MRM, Kaviski E, Detzel DHM. Evaluation of hydro-wind complementarity in the medium-term planning of electrical power systems by joint simulation of periodic streamflow and wind speed time series: a Brazilian case study. Renew Energy 2021;167:685–99. https://doi.org/10.1016/j.renene.2020.11.141.

[37] Cantão MP, Bessa MR, Bettega R, Detzel DHM, Lima JM. Evaluation of hydro-wind complementarity in the Brazilian territory by means of correlation maps. Renew Energy 2017;101:1215–25. https://doi.org/10.1016/j.renene.2016.10.012.

[38] de Souza Nascimento MM, Shadman M, Silva C, de Freitas Assad LP, Estefen SF, Landau L. Offshore wind and solar complementarity in Brazil: a theoretical and technical potential assessment. Energy Convers Manag 2022;270:116194. https://doi.org/10.1016/j.enconman.2022.116194.

[39] Antunes Campos R, Rafael do Nascimento L, Rüther R. The complementary nature between wind and photovoltaic generation in Brazil and the role of energy storage in utility-scale hybrid power plants. Energy Convers Manag 2020;221:113160. https://doi.org/10.1016/j.enconman.2020.113160.

[40] Gutsch M, Leker J. Global warming potential of lithium-ion battery energy storage systems: a review. J Energy Storage 2022;52:105030. https://doi.org/10.1016/j.est.2022.105030.

[41] Kumar A, Schei T, Ahenkorah A, Caceres Rodriguez R, Devernay J-M, Freitas M, et al. Hydropower. In: IPCC special report on renewable energy sources and climate change mitigation. Cambridge: Cambridge University Press; 2011. p. 1–496.

[42] Luiz-Silva W, Garcia KC. Sustainable future and water resources: a synthesis of the Brazilian hydroelectricity sector in face of climate change. Sustain Water Resour Manag 2022;8:120. https://doi.org/10.1007/s40899-022-00711-3.

[43] Cuartas LA, Cunha APM, Do A, Alves JA, LMP Parra, Deusdará-Leal K, et al. Recent hydrological droughts in Brazil and their impact on hydropower generation. Water (Basel) 2022;14:601. https://doi.org/10.3390/w14040601.

[44] de Oliveira Serrão EA, Silva MT, Ferreira TR, Freitas Xavier AC, dos Santos CA, Paiva de Ataide LC, et al. Climate and land use change: future impacts on hydropower and revenue for the amazon. J Clean Prod 2023;385:135700. https://doi.org/10.1016/j.jclepro.2022.135700.

[45] IEA. Towards common criteria for sustainable fuels. Paris. 2024.

[46] Krishnan S, Corona B, Kramer GJ, Junginger M, Koning V. Prospective LCA of alkaline and PEM electrolyser systems. Int J Hydrog Energy 2024;55:26–41. https://doi.org/10.1016/j.ijhydene.2023.10.192.

[47] Park J, Hwan Ryu K, Kim C-H, Chul Cho W, Kim M, Hun Lee J, et al. Green hydrogen to tackle the power curtailment: meteorological data-based capacity factor and techno-economic analysis. Appl Energy 2023;340:121016. https://doi.org/10.1016/j.apenergy.2023.121016.

[48] Esfandiari N, Aliofkhazraei M, Colli AN, Walsh FC, Cherevko S, Kibler LA, et al. Metal-based cathodes for hydrogen production by alkaline water electrolysis: review of materials, degradation mechanism, and durability tests. Prog Mater Sci 2024:144. https://doi.org/10.1016/j.pmatsci.2024.101254.

[49] Xia Y, Cheng H, He H, Wei W. Efficiency and consistency enhancement for alkaline electrolyzers driven by renewable energy sources. Commun Eng 2023;2:22. https://doi.org/10.1038/s44172-023-00070-7.

[50] Nguyen E, Olivier P, Pera M-C, Pahon E, Roche R. Impacts of intermittency on low-temperature electrolysis technologies: a comprehensive review. Int J Hydrog Energy 2024;70:474–92. https://doi.org/10.1016/j.ijhydene.2024.05.217.

[51] de Kleijne K, Huijbregts MAJ, Knobloch F, van Zelm R, Hilbers JP, de Coninck H, et al. Worldwide greenhouse gas emissions of green hydrogen production and transport. Nat Energy 2024. https://doi.org/10.1038/s41560-024-01563-1.

[52] Garcia GM, Oliva HS. Technical, economic, and CO2 emissions assessment of green hydrogen production from solar/wind energy: the case of Chile. Energy 2023;278:127981. https://doi.org/10.1016/j.energy.2023.127981.

[53] Patel GH, Havukainen J, Horttanainen M, Soukka R, Tuomaala M. Climate change performance of hydrogen production based on life cycle assessment. Green Chem 2024;26:992–1006. https://doi.org/10.1039/d3gc02410e.
[54] Schmidt J, Wehrle S, Turkovska O, Regner P. The EU additionality rule does not guarantee additionality. Joule 2024;8:553–6. https://doi.org/10.1016/j.joule.2024.02.003.
[55] Zilberman D. Indirect land use change: much ado about (almost) nothing. GCB Bioenergy 2017;9:485–8. https://doi.org/10.1111/gcbb.12368.
[56] BRASIL. LEI Nº 14.948, DE 2 DE AGOSTO DE 2024. Brasil. 2024.
[57] Weschenfelder F, Novaes Pires Leite de G, Araújo da Costa AC, Castro Vilela de O, Ribeiro CM, Villa Ochoa AA, et al. A review on the complementarity between grid-connected solar and wind power systems. J Clean Prod 2020;257:120617. https://doi.org/10.1016/j.jclepro.2020.120617.
[58] Kapica J, Canales FA, Jurasz J. Global atlas of solar and wind resources temporal complementarity. Energy Convers Manag 2021:246. https://doi.org/10.1016/j.enconman.2021.114692.
[59] Cai Q, Qing J, Zhong C, Xu Q, Liang Q-M. Temporal and spatial heterogeneity analysis of wind and solar power complementarity and source-load matching characteristics in China. Energy Convers Manag 2024;315:118770. https://doi.org/10.1016/j.enconman.2024.118770.